

Bulk and size-segregated aerosol composition observed during INDOEX 1999: Overview of meteorology and continental impacts

W. P. Ball,¹ R. R. Dickerson,^{1,2} B. G. Doddridge,² J. W. Stehr,² T. L. Miller,³ D. L. Savoie,⁴ and T. P. Carsey⁵

Received 21 April 2002; revised 7 December 2002; accepted 30 January 2003; published 30 May 2003.

[1] Bulk and size-segregated aerosol samples were collected from the NOAA R/V *Ronald H. Brown* as it cruised from Cape Town, South Africa, through the Indian Ocean and into the Bay of Bengal and Arabian Sea (February to April 1999; 33°S to 19°N). Throughout the Northern Hemisphere, aerosol loading was greater than in the Southern Hemisphere. Samples collected in air that had passed over India showed evidence of fossil fuel combustion, biomass burning, and eolian material, with elemental carbon (EC) dominating radiation absorption and the following relative contributions to the total mass of aerosol particles: ash 29%, nss-sulfate 22%, sea salt 15%, nitrate 9%, organic material 8%, ammonium 6%, and EC 5%. Careful examination of the coarse mode revealed substantial concentrations of nitrate, adequate to acidify sea salt aerosols north of the Intertropical Convergence Zone. Air that had passed over Arabia showed little evidence of biomass burning but had more acidity, mineral dust, and higher nitrate to sulfate ratios than air from India. High concentrations of mineral dust played a major role in radiation absorption; mean contributions to aerosol mass in Arabian air were: ash 38%, nss-sulfate 10%, sea salt 33%, nitrate 5%, organic material 4%, ammonium 1%, and EC 1%. From the ship we measured an average bulk aerosol concentration of 20 $\mu\text{g m}^{-3}$ in the marine boundary layer of the northern Indian Ocean. *INDEX TERMS*: 0365 Atmospheric Composition and Structure: Troposphere—composition and chemistry; 0305 Atmospheric Composition and Structure: Aerosols and particles (0345, 4801); 0322 Atmospheric Composition and Structure: Constituent sources and sinks; *KEYWORDS*: aerosol, nitrate, sulfate, ammonium

Citation: Ball, W. P., R. R. Dickerson, B. G. Doddridge, J. W. Stehr, T. L. Miller, D. L. Savoie, and T. P. Carsey, Bulk and size-segregated aerosol composition observed during INDOEX 1999: Overview of meteorology and continental impacts, *J. Geophys. Res.*, 108(D10), 8001, doi:10.1029/2002JD002467, 2003.

1. Introduction

[2] The lack of globally distributed aerosol data limits the ability to constrain chemical and radiative transport models. Aerosols have direct and indirect impacts on the atmosphere by altering the amount of incoming solar radiation and the optical properties of clouds. There are currently few measurements of aerosols in the tropics. The need to determine the extent of the impact of anthropogenic emissions in the tropics, the role of the Intertropical Convergence Zone (ITCZ) in pollutant transport, and the role of aerosols in climate change

were the rationale for the Indian Ocean Experiment (INDOEX) [Rhoads *et al.*, 1997; Lelieveld *et al.*, 2001].

[3] The Indian Ocean is bordered to the north by the polluted Indian subcontinent, an area of rapidly expanding industrialization, and to the south by the relatively unpolluted Southern Hemisphere. This provides the opportunity to compare the result of anthropogenic activities against a natural background. The background aerosol over ocean regions is primarily of marine origin and consists of sea salt particles and non-sea-salt (nss) sulfate produced by the oxidation of dimethyl sulfide (DMS) emitted from biological activity in the ocean [Fitzgerald, 1991]. The Indian subcontinent is becoming a larger source of pollution as the region has become more industrialized and the demand for fossil fuels has increased [Olivier *et al.*, 1994; Parashar *et al.*, 1998; Streets and Waldhoff, 1998, 1999; Dickerson *et al.*, 2002].

[4] The combustion of coal, oil, and other fossil fuels releases carbon dioxide, carbon monoxide, hydrocarbons, sulfur dioxide and various primary aerosols including fly ash, organic particles, and elemental carbon (EC), also called black carbon or soot. Biomass burning is a source of fine nss-potassium aerosol as well as nitrate, organic aerosol, elemental carbon, and ammonia [Andreae and

¹Department of Chemistry, University of Maryland, College Park, Maryland, USA.

²Department of Meteorology, University of Maryland, College Park, Maryland, USA.

³NOAA Pacific Marine Environmental Laboratory, Seattle, Washington, USA.

⁴Rosenstiel School of Marine and Atmospheric Science, University of Miami, Miami, Florida, USA.

⁵NOAA Atlantic Oceanographic and Meteorological Laboratory, Miami, Florida, USA.

Crutzen, 1997; Seinfeld and Pandis, 1998]. Animal waste and fertilizer are also major sources of atmospheric ammonia [Zhao and Wang, 1994]. In India, wood, animal dung and agricultural material are burned for fuel [Galanter et al., 2000; Lelieveld et al., 2001]. Smith [1988] suggested that cow dung, used extensively in India for domestic cooking fires, emits substantial amounts of SO₂. Elements commonly found in surface crustal material such as calcium and magnesium arrive in the atmosphere from wind blown (eolian) dust.

[5] On an earlier cruise, Savoie et al. [1987] observed high concentrations of nitrate, sulfate, and mineral dust over the Arabian Sea, and attributed these primarily to transport from the Arabian Peninsula, with transport from the Indian subcontinent becoming significant between dust outbreaks. Rhoads et al. [1997] confirmed the fundamental hypothesis of INDOEX by identifying a sharp gradient in pollutant concentrations across the ITCZ; they showed higher levels of continental species in the Northern Hemisphere with greatest aerosol optical depths and highest concentrations of mineral dust, sulfate, ammonium, nitrate, and trace gases in air blown directly off India. Other cruises [Lal et al., 1998; Johanson et al., 1999; Siefert et al., 1999; Parameswaran et al., 1999], aircraft flights [Lelieveld et al., 2001], and surface measurements at the Kaashidoo Climate Observatory (KCO) (5°N, 73°E) in the Maldives [Chowdhury et al., 2001] corroborated these general trends and showed that concentrations were much lower during the southwest monsoon. Dickerson et al. [1999] presented evidence from a PRE-INDOEX cruise of ozone destruction by halogen atoms in the marine boundary layer (MBL). The mechanism requires sea salt particles with a pH below 6, and here we examine the acid-base chemistry of those particles.

[6] This paper presents aerosol measurements made onboard the NOAA R/V *Ronald H. Brown* during the winter monsoon (dry) season, when the prevailing winds carry air from the Indian subcontinent and Arabia to the Indian Ocean [Parsons and Dickerson, 1999]. We discuss detailed observations of aerosol composition in the context of meteorological conditions (section 2.1) then examine correlations between aerosol species and between aerosols and trace gases to provide insight into the origin of the pollutants (section 3.1). The wavelength dependence of radiation absorption by the bulk aerosol is examined to determine the dominant absorbing species (section 3.2). In size-segregated samples, special attention is paid to the coarse aerosol, where the nitrate is expected to reside (section 3.3).

2. Experimental Techniques

[7] Both high-volume and low-volume impactors were used during INDOEX because of their complementary properties. As employed, high-volume impactors have better collection efficiency for large particles (aerodynamic diameter >1 μm) and better detection limit than low-volume impactors [Howell et al., 1998]. High-volume impactors have better size resolution for particles in the coarse mode (calcium, sea salt and the nitrate that absorbs onto it), while the low-volume impactors have better size resolution for fine particles (aerodynamic diameter <1 μm). Two high-volume Sierra Instruments aerosol samplers, one cascade

impactor and one bulk collector were used. These high-volume impactors collect a large mass of aerosol, but have less precise size segregation compared to low-volume impactors, such as those used by Quinn et al. [2002]. The samplers were located at the top of a 10-m walkup tower located at the bow of the ship, a total of 15-m above sea level. Filters were changed twice a day at 6 AM and 6 PM local time, to separate daytime from nighttime samples. To avoid contamination, sampling was stopped when the wind direction was from the ship or wind speed was less than 3 m s⁻¹. The sectoring restrictions reduced the collection time by an average of 15 (±10)% for each sampling period.

[8] The cascade impactor consisted of five stages that segregated the total particulate material into six size fractions. Slotted Whatman 41 paper filters were used as the impaction surface. The aerodynamic cut-points (d₅₀ values) for stages one to five were 7.2, 3.0, 1.48, 0.96, and 0.48 μm respectively [Pszenny, 1992]. A backup 20 by 25 cm Whatman 41 filter collected particles with mean aerodynamic diameter <0.48 μm. The bulk sampler consisted of a single 20 by 25 cm Whatman 41 filter. Ambient air was drawn through the samplers at an average sample flow rate of 1.1 m³ min⁻¹ and 1.5 m³ min⁻¹ (25°C and 1 ATM) for the cascade impactor and bulk sampler respectively. Whatman 41 filters have mass collection efficiencies of greater than 90% for sulfate and greater than 95% for sea salt and nitrate [Savoie et al., 1992]. Whatman 41 filters are known to collect HNO₃ vapor with high efficiency, we consider our measured nitrate concentrations to be those of total inorganic nitrate (particulate nitrate plus gaseous HNO₃ [Savoie et al., 1989]). However, the concentration of gaseous HNO₃ in the near-surface marine boundary layer is typically around 20% or less of the total nitrate [Savoie and Prospero, 1982].

[9] The bulk sampler collected aerosol particles more efficiently than the cascade impactor. For sea salt particles, the bulk sampler collected 35% more mass than the sum of the cascade stages; for species carried on mineral dust, such as calcium, the difference was 40%. The high collection efficiency of the bulk samplers for coarse mode particles yields higher total nitrate concentrations than other methods used during the cruise. For species carried on the fine aerosol, such as sulfate, potassium and ammonium, the concentration measured by the bulk sampler was only about 10% greater than the sum of the cascade samples. Cascade impactor samples presented in this paper averaged 12% more ammonium than samples collected simultaneously by PMEL [Quinn et al., 2002], but this difference is within the combined experimental uncertainty of the two techniques.

[10] We cut 47-mm diameter portions from the bulk and cascade backup filter papers and quarter sections of the slotted filter papers of the cascade impactor for analysis. Remaining filters were placed into individual polyethylene bags and refrigerated. The cut portions of the filters were extracted using water and methanol. The resulting solutions were analyzed by ion chromatography for sodium, chloride, nitrate, sulfate, ammonium, potassium, calcium and magnesium [Quinn et al., 1998]. Non-sea-salt (nss) concentrations of potassium, magnesium, calcium and sulfate were calculated from their constant ratios in seawater [Keene et al., 1986]. Blanks were prepared in the same manner as the samples, except air was not drawn through them. Detection

Table 1. Detection Limits for Aerosol Components Calculated From Twice the Standard Deviation of the Filter Blank, With Corrections for Portion of Filter Used^a

Component	Bulk, $\mu\text{g m}^{-3}$	Cascade per Stage, $\mu\text{g m}^{-3}$
Sodium	0.074	0.029
Chloride	0.071	0.077
Sulfate	0.042	0.013
nss-Sulfate	0.061	0.020
Potassium	0.003	0.002
nss-Potassium	0.029	0.003
Calcium	0.005	0.020
nss-Calcium	0.008	0.021
Magnesium	0.003	0.005
nss-Magnesium	0.011	0.008
Nitrate	0.020	0.007
Ammonium	0.052	0.030

^aBased on average sampling volume of 880 m³ for bulk samples; 670 m³ for cascade samples.

limits were defined as twice the standard deviation of the blanks (Table 1). Additional uncertainties due to errors in analytical technique and flow rate are estimated to be 30%. Samples from alternate days were analyzed on the ship and the remaining samples were analyzed at the Pacific Marine Environmental Laboratory (PMEL), Seattle, Washington upon return to the United States. The difference between

samples analyzed immediately and those analyzed several months later was within the estimated overall uncertainty in the technique.

[11] A subset of twenty bulk samples from various points along the cruise was selected for additional analysis. Of the twenty samples, three were from the Southern Hemisphere. The remaining samples were selected in order to have at least three samples from each Northern Hemisphere regime (section 3.1) and comprised half of the total samples collected in the Northern Hemisphere. These samples were analyzed following the cruise for ash content and absorption spectra. Ash is defined as the mass remaining after high-temperature combustion [Savoie *et al.*, 1987]. Compounds such as sulfates, nitrates, sodium chloride, and organic species are lost in combustion, leaving refractory materials such as mineral dust and fly ash. These twenty samples were also analyzed at the University of Miami for sodium by atomic absorption, ammonium by automated colorimetry and sulfate and nitrate using ion chromatography [Maring *et al.*, 2000].

[12] The spectrally resolved measurements of aerosol absorbance were made using an Optronic OL 740A Spectroradiometer with an OL 740-70 Diffuse Reflectance Attachment (DRA). The DRA is an integrating sphere with three ports. One port is for the light beam entering from the

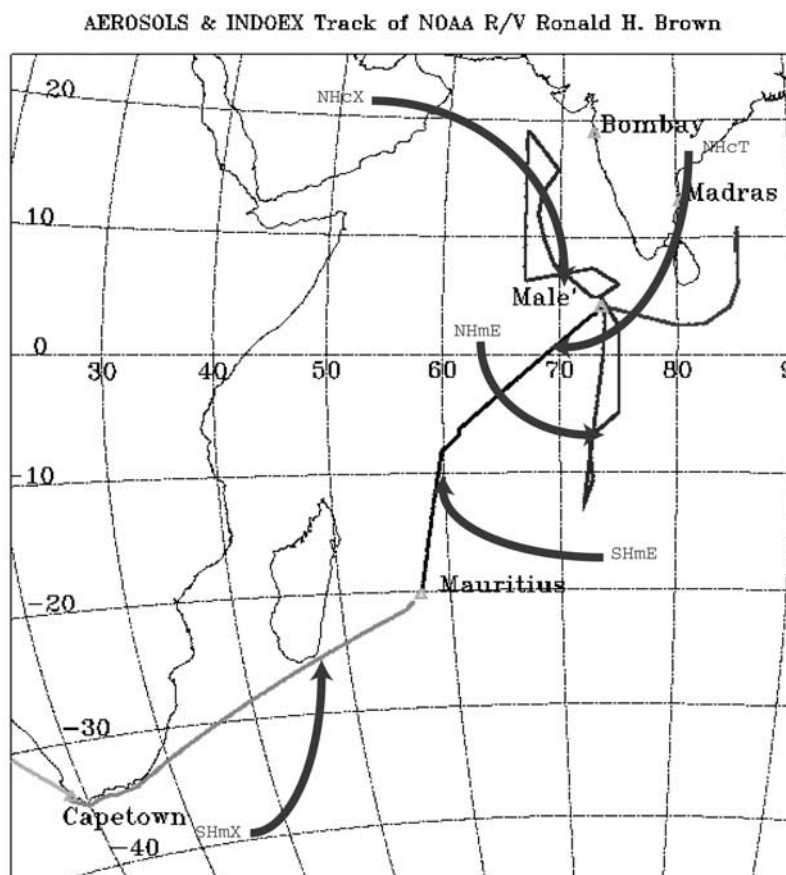


Figure 1. Cruise track (thin lines) of the R/V *Ronald H. Brown* during the 1999 INDOEX campaign. The ship traveled from Cape Town to Mauritius, to Malé, into the Arabian Sea, south across the ITCZ back north into the Bay of Bengal, and back to Malé. Thick arrows represent air mass average back trajectories calculated with Hy-SPLIT as indicated in the text.

Table 2. Time Line for NOAA R/V *Ronald H. Brown*: INDOEX 1999

DOY	Date	Action	Atmospheric Conditions
42	11 Feb	depart Cape Town (34°S, 8°E) begin AEROSOLS Leg 2	SHmX regime
47	16 Feb	arrive SHmE regime, (30°S, 35°E)	transition to SHmE regime 0500 ^a wind shifts S to SE 2035 UTC light showers
48	17 Feb		0200–0853 drizzle to rain showers
49	18 Feb		1614 rain showers
51	20 Feb	arrive Mauritius (20°S, 57°E)	continued SHmE
53	22 Feb	depart for Malé, Maldives begin INDOEX Leg 1	1836 rain showers continued SHmE
54	23 Feb		0745–1839 light rain to rain showers 2044 rain 2245–2315 moderate rain shower
58	27 Feb	entering ITCZ area	1340 lightning to NE transition to NHcT, sharp increase in all pollutants 2053, 2253, 2345, lightning in area 2459 squall within 5 km
59	28 Feb	cross ITCZ (1°N, 70°E)	1809 showers 2001 lightning to SSE
60	1 Mar	arrive Malé, Maldives (4°N, 73°E)	continued NHcT
63	4 Mar	depart Malé on INDOEX Leg 2	continue polluted NHcT regime haze observed frequently high aerosol light scattering
68	9 Mar	entering NHcX regime	cooling temperatures wind shifting from NE to N at 0000 UTC (15°N, 69°E) light scattering decreasing
70	11 Mar	arrive farthest point N (19°N, 67°E) turn S and begin Leg 2b	continued clear skies and NHcX regime
71	12 Mar	mixed air masses	entering NHc regime atmospheric composition characteristic of mixed NHcT and NHcX air
75	16 Mar		1540 to 1550 rain showers tapering to drizzle 1908 and 2103 lightning to SSE
76	17 Mar	enter ITCZ region	1800 enter NHmE regime 1900 lightning to SSE 2100 lightning to S and SW 1555 rain 1900 lightning to SSE
77	18 Mar	refuel at Diego Garcia 0600–1200	1800 enter SHmE regime, cleaner air
78	19 Mar	1400 reach farthest point S (13°S, 72°E) turn N	0120 showers 1300 drizzle on ship 1928 lightning to NNE 2129 light rain shower
79	20 Mar		0440 light rain 1100 transition to NHmE air 2000 light rain shower 2135 lightning to NNE
80	21 Mar		1900 lightning to N NHmE regime 2100 lightning NNE 2320 lightning in squall line to N
81	22 Mar		0000 nearby showers to N 0100 nearby showers to E 0615 light rain 1430 and 1900 lightning
82	23 Mar	arrive Malé	
85	26 Mar	end Leg 2b depart Malé begin INDOEX Leg 3, heading into Bay of Bengal	NHcT regime, polluted and hazy
88	29 Mar		heavy pollution, haze
89	30 Mar	arrive farthest point north at 0100 (11°N, 85°E) and return to Malé	end sampling
92	2 Apr	arrive Malé, end Leg 3	no sampling

^aAll times are UTC.

spectroradiometer. The other two ports on the opposite side of the sphere are for the substrates to be analyzed. To ensure reproducibility, measurements of all samples and blanks were made using the same sample port. The other sample

port was kept covered with a white Teflon film (supplied by the manufacturer) with reflective characteristics comparable to that of the interior surface of the integrating sphere. For this study, the spectroradiometer was operated under com-

Table 3. Average ($\pm\sigma$) Bulk Aerosol Concentrations ($\mu\text{g m}^{-3}$) by Regime

	SHmX	SHmE	NHcT	NHcX	NHc	NHmE
Day of year	42–47.6	47.6–57, 78	58–60, 63–67, 85–88	68–70	71–76.5	76.75–77 79–82
Number of samples	6	13	17	4	10	5
Na ⁺	4.47 \pm 1.00	2.56 \pm 0.83	1.17 \pm 0.27	3.31 \pm 0.56	2.29 \pm 0.28	4.00 \pm 0.99
Cl ⁻	7.08 \pm 1.69	3.84 \pm 1.26	1.82 \pm 0.50	5.13 \pm 0.91	3.01 \pm 0.32	6.30 \pm 1.02
Total SO ₄ ²⁻	1.26 \pm 0.16	1.00 \pm 0.18	4.66 \pm 0.73	2.16 \pm 0.21	3.53 \pm 0.31	3.01 \pm 0.91
nss SO ₄ ²⁻	0.16 \pm 0.10	0.36 \pm 0.10	4.36 \pm 0.73	1.33 \pm 0.12	2.96 \pm 0.30	2.01 \pm 0.72
total K ⁺	0.16 \pm 0.04	0.09 \pm 0.03	0.25 \pm 0.04	0.12 \pm 0.02	0.26 \pm 0.02	0.26 \pm 0.09
nss K ⁺	<0.01	<0.01	0.21 \pm 0.04	<0.01	0.18 \pm 0.02	0.11 \pm 0.05
Total Ca ²⁺	0.25 \pm 0.11	0.12 \pm 0.04	0.26 \pm 0.06	0.67 \pm 0.05	0.62 \pm 0.14	0.42 \pm 0.10
nss Ca ²⁺	0.08 \pm 0.09	0.02 \pm 0.10	0.22 \pm 0.06	0.55 \pm 0.04	0.53 \pm 0.13	0.27 \pm 0.06
Total Mg ²⁺	0.47 \pm 0.14	0.26 \pm 0.09	0.14 \pm 0.03	0.33 \pm 0.04	0.29 \pm 0.04	0.43 \pm 0.11
nss Mg ²⁺	0.014 \pm 0.056	<0.01	0.02 \pm 0.01	<0.01	0.06 \pm 0.01	0.03 \pm 0.01
NO ₃ ⁻	0.04 \pm 0.04	0.13 \pm 0.03	2.04 \pm 0.37	1.27 \pm 0.17	2.34 \pm 0.26	1.07 \pm 0.46
NH ₄ ⁺	n.a.	0.07 \pm 0.02	1.53 \pm 0.31	0.36 \pm 0.02	1.27 \pm 0.19	0.68 \pm 0.31
Ash	<0.01	0.34 \pm 0.10	5.58 \pm 0.91	10.37 \pm 4.14	4.01 \pm 2.09	1.91
Organic carbon	0.26 \pm 0.07	0.16 \pm 0.04	1.05 \pm 0.16	0.65 \pm 0.13	0.94 \pm 0.23	0.29 \pm 0.06
Elemental carbon	0 \pm 0	0.04 \pm 0.04	0.97 \pm 0.17	0.21 \pm 0.07	0.45 \pm 0.11	0.14 \pm 0.03
Total mass	14.5	9.0	19.7	25.8	18.8	18.3

puter control to supply a light beam with wavelengths ranging from 300 to 1100 nm at 10 nm intervals with a bandwidth of 5 nm. At each wavelength, readings of reflected light intensity were taken until three successive readings were all within 0.5% of one another. The average of these three readings was then recorded as the reflectance measurement for that wavelength.

[13] The samples used in this analysis were 25-mm diameter punches from the high-volume Whatman-41 bulk filter samples used for measurements of the major ions and ash. Blank Whatman-41 filters are white and highly reflective (greater than 70% diffuse reflectance over the spectrum) and provide a good background for the measurements. The aerosol absorption in the filter samples was determined by comparison of the sample reflectance to the reflectance of blank filters. To ensure proper comparisons, sample absorbances were based on comparisons only with corresponding blanks that were run during the same day.

[14] Aerosol samples collected by the Institute for Tropospheric Research, Leipzig, Germany provide the elemental and organic carbon data. All aerosol samplers on the ship followed the same sampling protocol (e.g., sample start/end time, sectoring for wind speed and direction). Details of the analytical techniques used for the carbon data and further INDOEX results are presented by *Neusuess et al.* [2002]. Meteorological measurements were provided by NOAA and obtained using the Woods Hole Improved Meteorological (IMET) sensor set. These were located on several towers on the ship at altitudes ranging from 10 to 30 m above the sea surface.

[15] From 11 February to 28 March 1999, bulk and size segregated aerosol samples were collected aboard the NOAA R/V *Ronald H. Brown* in the Indian Ocean. The cruise track from Cape Town, South Africa to the Maldives is shown in Figure 1.

[16] The differences in the aerosol and trace gas data mirror differences in the origin of the air masses as characterized by their back trajectories. An “air mass” is a widespread body of air that resides over a uniform surface long enough to acquire consistent physical properties over a large horizontal area; these generally fall into three main types classified by thermal properties: Polar (P), tropical (T), and equatorial (E) [*Ahrens, 2000; Glickman, 2000*].

They can be further subdivided, according to moisture content, into maritime (m) and continental (c); for the INDOEX environment, air from outside the tropics was not “polar” in nature, and has been labeled extratropical (X). An air mass is characterized by its vertical structure and stability, and is modified in transit; the concept has long been useful in weather forecasting [*Rossby, 1932*]. Air masses can also develop uniform chemical properties, and this concept can be useful in describing broad categories of meteorological conditions with characteristic air chemistry [e.g., *Rhoads et al., 1997*]. These air masses, or meteorological regimes, tend to recur.

[17] As the ship sailed through the Indian Ocean it encountered several distinct air masses or meteorological regimes, and the composition of the air reflected the atmospheric circulation characteristic of these regimes (Table 2). We identified air masses using meteorological analyses on the basis of a physically initialized GCM [*Krishnamurti et al., 1997*] and 6-day back trajectories. HYSPLIT [*Draxler, 1991*] was used to calculate three dimensional back trajectories at altitudes corresponding to 950, 850 and 500 hPa above the ship’s position at 0000, 0600, 1200, and 1800 UTC for each day of the cruise. The depth of the marine boundary layer varied from 500 to 2000 m, and these calculated trajectories indicate the synoptic situation and general origin of the air mass sampled, not the literal path traversed by an air parcel. The complete set of back trajectories can be found at <http://saga.pmel.noaa.gov/indoex/traject/index.html>.

[18] Precipitation changes the nature of an air mass in several ways. Soluble species, including much of the fine-mode aerosol, are removed from the lower troposphere. Vertical mixing, especially in convective clouds, redistributes pollutants, and because such sub-grid-scale processes must be parameterized in global analyses, back trajectories are only reliable until they intersect convection. Interpretation of the relationship of meteorology and air composition must consider these processes. The analyses of precipitation [*Jha and Krishnamurti, 1999*] help indicate the useful limit of computed back trajectories. For this paper, classification of meteorological regimes is little affected by precipitation because during the boreal spring, large-scale subsidence suppresses precipitation. Rain would remove all ionic

Table 4. Average ($\pm\sigma$) Trace Gas Concentrations and Meteorological Conditions by Regime

	SHmX	SHmE	NHcT	NHcX	NHc	NHmE
Day of year	42–47.6	47.6–57, 78	58–60, 63–67, 85–88	68–70	71–76.5	76.75–77 79–82
Number of samples	6	13	17	4	10	5
Ozone, ppb	18 \pm 1	12 \pm 1	25 \pm 2	47 \pm 1	27 \pm 2	16 \pm 4
CO, ppb	47 \pm 1	58 \pm 4	149 \pm 8	134 \pm 1	124 \pm 4	90 \pm 7
Wind speed, m s ⁻¹	5.6 \pm 0.6	2.9 \pm 0.5	2.9 \pm 0.4	7.0 \pm 0.2	2.8 \pm 0.4	3.4 \pm 1.1
Wind direction, deg	174 \pm 23	100 \pm 32	42 \pm 23	353 \pm 7	334 \pm 28	300 \pm 21
RH, %	69 \pm 4	76 \pm 2	75 \pm 1	70 \pm 1	75 \pm 1	78 \pm 1
T, C	22 \pm 1	27 \pm 0.5	28 \pm 0.2	25 \pm 0.4	28 \pm 0.1	28 \pm 0.2
Sea surface T, °C	25.3 \pm 2.3	28.2 \pm 0.9	29.0 \pm 0.3	27.3 \pm 0.6	28.6 \pm 0.7	
$\frac{\text{NH}_4^+}{\text{NO}_3^- + 2\text{SO}_4^{2-}}$ ^a	NA ^b	NA	0.64	0.43	0.69	0.64
$\frac{\text{NH}_4^+ + \text{K}^+}{2\text{SO}_4^{2-}}$ ^a	NA	NA	0.95	0.75	1.20	0.97

^aBy mole.

^bNA, not available.

species on aerosols with essentially the same efficiency; even EC would be rained out because it was generally mixed internally (S. A. Guazzotti et al., Characterization of pollution outflow from India and Arabia: Biomass burning and fossil fuel combustion, submitted to *Journal of Geophysical Research*, 2002). This indicates that correlation analyses would be little affected by precipitation. The ship encountered substantial rain south of the ITCZ between 17 and 23 February (days 48–54), but thereafter only near the ITCZ and during a locally intense thunderstorm on the Bay

of Bengal on 28 March (day 87). Means and standard deviations of aerosol concentrations for each regime are summarized in Table 3, trace gas measurements and meteorological conditions are summarized in Table 4.

[19] Six meteorological regimes were encountered during the cruise. These regimes have been labeled Southern Hemisphere maritime extratropical (SHmX), Southern Hemisphere maritime equatorial (SHmE), Northern Hemisphere maritime equatorial (NHmE), Northern Hemisphere continental tropical (NHcT), Northern Hemisphere conti-

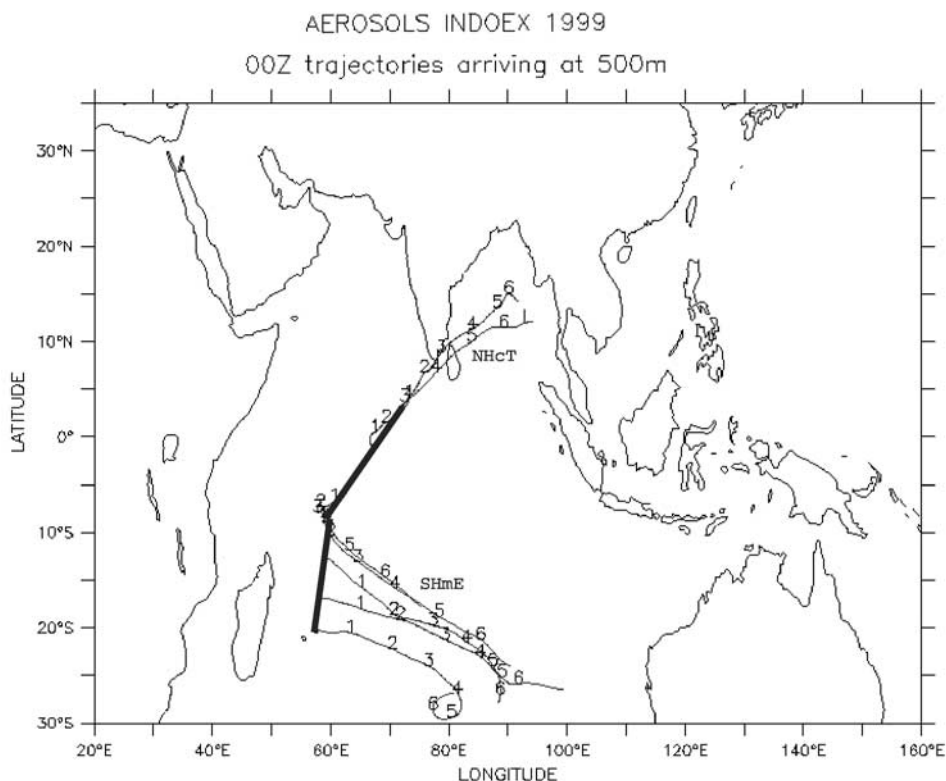


Figure 2. Back trajectories (thin lines) that arrived at the ship on 00Z each day at 500 m during the first leg of INDOEX. The numbers in each trajectory show where the air masses were on that number of days (24 hour periods) back from arrival at the ship position (cruise track is thick line). As the ship crossed the ITCZ and entered the meteorological Northern Hemisphere winds shifted from SE to NE.

nenal extratropical (NHcX) and Northern Hemisphere continental (NHc). These meteorological groupings were determined by examining clusters of back trajectories, considering primarily on the latitude and longitude and distance, corresponding to horizontal wind direction and speed. Local meteorological conditions (T, RH, WD, WS), and pollutant concentrations, were also examined, but back trajectories alone were generally adequate to establish changes in air masses (Figures 1 and 2). To confirm the distinctiveness of the regimes, we examined the CO concentrations. Distributions of CO (mean $\pm\sigma$) in no two regimes overlap (Table 4). If the standard deviations are converted to standard deviations of the means by dividing by the number of samples, the significance greatly exceeds 95% confidence, demonstrating that the chemical nature of each air mass is discrete.

[20] The SHmX back trajectories were relatively long and went from the south then around to the southwest. SHmE trajectories pointed to the SE, but as the ship crossed the ITCZ and entered the meteorological Northern Hemisphere the back trajectories moved to the NE and crossed over India; these were classified NHcT (Figure 2). If back trajectories in the Northern Hemisphere remained over the ocean for 6 days or more, then they were classified NHmE. When trajectories passed over the Arabian Peninsula, the air mass was classified as NHcX, or simply NHc as described below.

[21] As the Brown departed Cape Town, South Africa and headed east, we encountered relatively strong surface winds (7 m s^{-1} average) in the SHmX regime with breezes arriving at the ship from the south. Farther back along the trajectories, winds veered westerly, steered by the persistent subtropical anticyclone in the South Atlantic. Back trajectories from this period typically show long traces across the south Indian and Atlantic Oceans with the air parcels spending much of their time in the zonal flow of the remote marine free troposphere. In this subtropical air, temperatures were cool and humidities low (23°C , 69%).

[22] A large increase in average air and sea surface temperatures was seen as we left the SHmX and entered the SHmE regime; easterly surface winds prevailed. The southeasterly trade winds dominate most of the back trajectories for this period (Figure 2). Shipboard observations and rawinsondes launched from the ship indicate winds aloft from the east; trajectories remain entirely over the southern Indian Ocean. Several rain showers met the ship as we approached Mauritius (20°S , 57°E).

[23] As the ship left Mauritius on the first leg of INDOEX, we remained in the SHmE regime with locally high temperatures, relative humidities (27°C , 76% on average) and weak winds leading to air that had been cleansed by long, slow travel over the equatorial Indian Ocean. Near 7°S the ship approached the general area of cyclones associated with the ITCZ. The ITCZ was sharply defined at 1°N on 28 February (day 59). Widespread deep convection was encountered, but surface winds were weak. Back trajectories crossed southern India 2–4 days upwind as we encountered NHcT air (Figure 2). On 1 March (day 60), the ship arrived at Malé in the Maldives.

[24] The hazy NHcT air mass persisted as the ship departed Malé to start INDOEX Leg 2. The NHcT air mass was characterized by weak, NNE winds (3 m s^{-1}), high

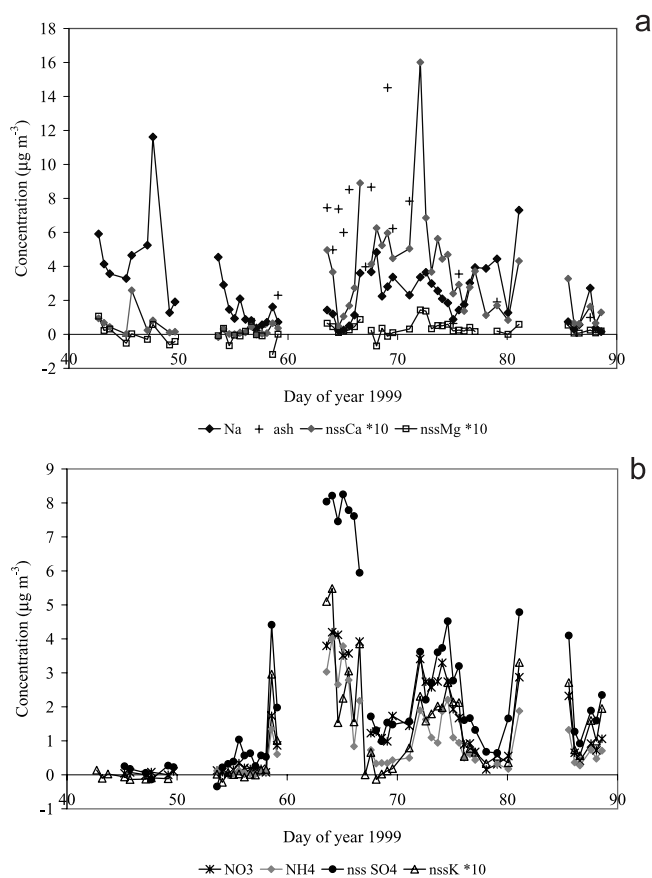


Figure 3. Concentration of aerosol samples collected during the cruise of NOAA R/V *Ronald H. Brown* during INDOEX as a function of the day of 1999. Each point represents the concentration measured over a 12 or 24-hour sampling period and corresponds to the start time (UTC) of the sample. The three gaps in the data are from days the ship was in port. (a) The time series of sea salt and crustal material, including sodium, nss-magnesium, nss-calcium and ash. (b) The time series of pollution components, nss-sulfate, nss-potassium, nitrate and ammonium. The Southern Hemisphere (days 47–57, 16–26 February) has sea salt as the principal aerosol component. The Northern Hemisphere has increased continental influence as evidenced by the high levels of pollution and crustal components. After the ITCZ was crossed on day 58 (27 February), the ship remained in the meteorological Northern Hemisphere except for days 77 and 78 (18 and 19 March).

humidity (75%), air temperatures (28°C), and sea surface temperatures, SST, (29°C). On 8 March (day 67) the air mass began the transition from NHcT to NHcX with RH, air temperature and SST dropping, and surface winds backing from NE to N. In this extratropical air mass, the average temperature was 3°C below that of the NHcT regime, and wind speeds were twice as high. Back trajectories show the origin of the air shifting from India to the area around the Persian Gulf, including Iraq, Iran, and the Saudi Arabian peninsula.

[25] The Brown reached its most northerly point (19°N), the latitude of Bombay, on 11 March (day 70) and then turned south. On 12 March, low-level back trajectories

Table 5. Correlation Coefficients, r , for Carbon Monoxide, Ozone, Aerosols and Meteorological Parameters, AEROSOLS 99 Leg 2 and INDOEX Legs 1–3

	Ozone	CO	Na ⁺	NH ₄ ⁺	nssK ⁺	nssMg ²⁺	nssCa ²⁺	Cl ⁻	NO ₃ ⁻	SO ₄ ²⁻	nssSO ₄ ²⁻	Ash	OC	EC	WS	RH	T
Ozone	1																
CO	0.60	1															
Na ⁺	0.14	-0.35	1														
NH ₄ ⁺	0.31	0.66	0.10	1													
nssK ⁺	0.32	0.74^a	-0.19	0.94	1												
nssMg ²⁺	0.24	0.22	0.20	0.45	0.36	1											
nssCa ²⁺	0.64	0.38	0.19	0.47	0.43	0.55	1										
Cl ⁻	0.14	-0.36	0.96	0.01	-0.23	0.07	0.17	1									
NO ₃ ⁻	0.58	0.72	-0.02	0.91	0.88	0.58	0.71	-0.12	1								
SO ₄ ²⁻	0.46	0.66	0.07	0.88	0.90	0.44	0.51	0.06	0.91	1							
nssSO ₄ ²⁻	0.41	0.73	-0.18	0.88	0.92	0.40	0.45	-0.18	0.91	0.97	1						
Ash	0.84	0.51	0.11	0.17	0.16	0.28	0.72	0.07	0.40	0.32	0.29	1					
OC	0.16	0.45	-0.19	0.51	0.54	0.34	0.14	-0.12	0.65	0.68	0.70	0.14	1				
EC	0.13	0.85	-0.45	0.64	0.71	0.16	-0.12	-0.43	0.55	0.69	0.74	0.43	0.73	1			
WS	0.38	-0.17	0.45	-0.12	-0.28	0.05	0.23	0.48	-0.06	-0.06	-0.17	0.33	-0.23	-0.27	1		
RH	-0.22	0.06	0.12	0.22	0.15	0.13	-0.08	0.08	0.08	0.14	0.12	-0.10	0.14	0.02	-0.29	1	
T	-0.10	0.43	-0.47	0.22	0.44	0.08	0.12	-0.44	0.34	0.26	0.35	-0.18	0.20	0.18	-0.55	0.23	1

^aValues in bold represent correlation coefficients significant at the 98% confidence level.

indicate that the regime was still NHcX, but meteorological variables and concentrations of trace species are similar to those of the NHcT regime. The synoptic-scale fields used to construct back-trajectories lack the resolution to resolve mesoscale processes, but direct measurements indicate that winds in the lower free troposphere and the sea breeze circulation along the Indian coast mixed air from India into this air mass, labeled NHc.

[26] This NHc regime persisted, but passage over the Arabian Sea and northern Indian Ocean modified the air mass, giving it an increasing maritime character and lower pollutant concentrations. By 17 March, the nature of the air mass was thoroughly NHmE with high temperatures and RH. In mid March, the ITCZ lay well into the Southern Hemisphere at about 12°S. A brief encounter with SHmE air occurred on 18 and 19 March with pollutants reaching a local minimum as the ship arrived at its most southern point of this leg, 13°S. As the ship reversed course, widespread convection and rain accompanied the return to Malé in generally NHmE air.

3. Results and Discussion

3.1. Bulk Aerosol Samples

[27] Time series (Figure 3a) show that sea salt, represented by sodium, dominates the aerosol component in the Southern Hemisphere, on days 42–57 of 1999 (11–26 February); the small spike in Ca on day 46 (15 February) resulted from wind catching the edge of the African continent [Quinn *et al.*, 2002]. As the ship crossed the Inter-tropical Convergence Zone (ITCZ) on 27 February (day 58), the concentrations of mineral dust components nss-calcium, nss-magnesium, and ash increased and remained high throughout much of the ship’s course in the Northern Hemisphere. Continental aerosol, and not sea salt, then dominated the mass of the aerosol.

[28] Time series (Figure 3b) also show that nitrate, nss-sulfate and ammonium were low (often below the detection limit) in the Southern Hemisphere, days 42–57 (11–26 February). As the ITCZ was crossed on day 58 (27 February), and Northern Hemisphere air was sampled, the concentrations of aerosols from anthropogenic origins

(nitrate, nss-sulfate, and nss-potassium) increased by an order of magnitude. Substantial variability was observed as the ship encountered air from India or the Arabian Peninsula that had been over the ocean for varying amounts of time.

[29] To help determine the sources of the pollution observed over the Indian Ocean, correlation coefficients were calculated for every pair of aerosol species, carbon monoxide, ozone, elemental carbon, organic carbon, temperature, relative humidity and wind speed for the entire data set (Table 5). Strong positive correlations suggest, but do not prove a common source and/or colocated sources. Lack of correlation shows separate sources or removal processes, but what correlation coefficient is required for statistical significance?

[30] The meteorological synoptic conditions establish the number of independent variables or the degrees of freedom

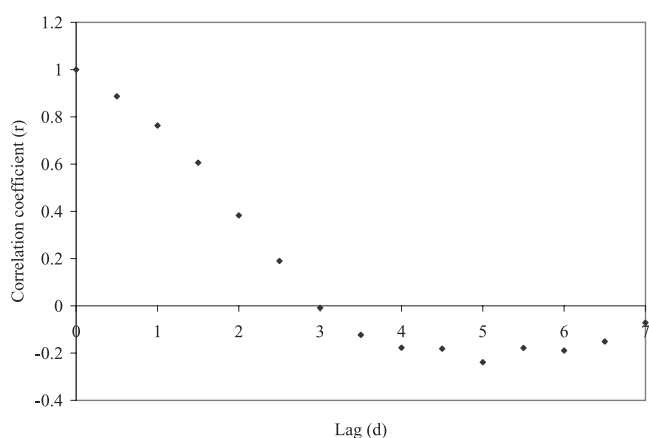


Figure 4. Autocorrelation for nss-sulfate. The correlation coefficient, r , for the time series of aerosol nss-sulfate concentrations regressed against the same series shifted (lagged) by time indicated on the x axis. For zero time lag, r must be unity. After about 2.5 days the correlation coefficient is near zero, indicating that, on average, the ship remained in a given air mass or synoptic situation 2–3 days during INDOEX 1999.

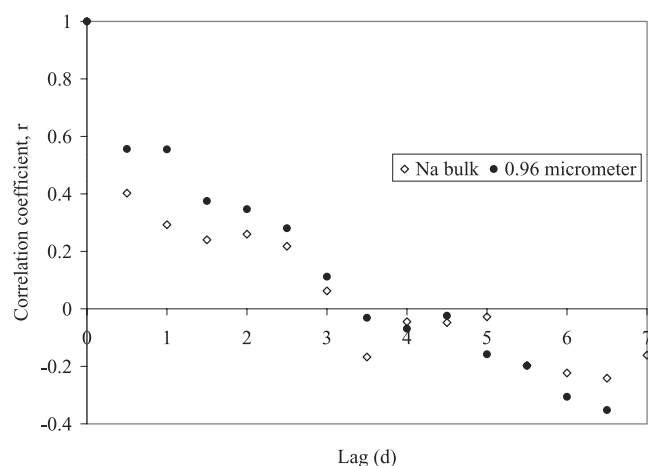


Figure 5. Autocorrelation for sodium. The correlation coefficient, r , for the time series of aerosol sodium concentrations regressed against the same time series shifted (lagged) by the time indicated on the x axis. For zero time lag, r must be unity. For the concentration of bulk (total) sodium, the correlation coefficient is reduced substantially after 12 hours and fluctuates around zero after 1 day, indicating a low degree of autocorrelation after 24 hours. For sodium on smaller particles (a mean diameter around 0.96 μm) the value of r drops off more slowly, indicating a higher degree of autocorrelation, due perhaps to a longer lifetime in the MBL for sea salt particles in this size range.

for our data set (for species with lifetime similar to or longer than the timescale of changes in synoptic situation). If multiple observations are made within an air parcel of uniform meteorological characteristics and chemical composition then the number of degrees of freedom must be less than the number of observations. The persistence of meteorological synoptic situations and the degree of autocorrelation in our data were investigated by calculating for each species the correlation coefficient of the original time series with the time series lagged by 0–84 hours in 12 hour increments. As an example, the degree of autocorrelation for nss-sulfate (Figure 4) is still high after 12 hours ($r = 0.9$) but decreases substantially after 2 days and approaches zero after 3 days. This pattern was typical for species on fine aerosol particle. On the basis of this analysis, a synoptic event was determined (conservatively) to last on average 3 days during the cruise. The number of different synoptic events for the 34 days of sampling was estimated to be 11 (34 sampling days/3 day synoptic events) with 9 degrees of freedom. The two-tailed test for statistical significance indicates that a correlation coefficient of 0.602 is significant at the 95% confidence level. For this paper, a strong correlation is defined as one in which r exceeds 0.71 such that half or more of variability can be attributed to the independent variability, i.e., r^2 exceeds 0.5. A correlation coefficient of 0.71 is statistically significant with greater than 98% confidence for 9 degrees of freedom.

[31] Beginning with the strongest positive correlations (Table 5), the coefficient for sodium and chloride (0.96) reflects that sea salt is the dominant source; the average of the Na^+/Cl^- molar ratio is 1.1, somewhat depleted in chloride relative to sea salt (Na^+/Cl^- in ocean water is approximately

0.86). The next strongest correlation is between nss-potassium and ammonium. Biomass burning produces potassium and ammonia, although the collocation of animal husbandry and agricultural burning could contribute to the strong correlation. Nss-potassium, a good marker for biomass burning, also demonstrates strong positive correlations with nitrate, carbon monoxide, sulfate and elemental carbon. Nss-sulfate, generally a good marker for fossil fuel combustion, shows strong positive correlations with carbon monoxide, ammonium, nss potassium, nitrate, organic carbon, and elemental carbon. Fossil fuel combustion is known to release nitrate-forming oxides of nitrogen, and inefficient or incomplete combustion of fossil fuels produces carbon monoxide and carbon-containing aerosols. The correlation of sulfate with ammonia may originate from independent, colocated sources, but it may be the result of ammonia and sulfur released from burning cow dung or from reaction of ammonia with sulfate in transit. This correlation matrix is unable to assign combustion of biomass or fossil fuel as the primary source of EC, suggesting that either a combination of the two or some unaccounted-for source dominates.

[32] Wind speed and sea salt aerosol are positively correlated, but r is only 0.45–0.48. Atmospheric sea salt particles can be produced at low to moderate wind speeds [Erickson and Duce, 1988]. Nss-calcium, nss-magnesium and ash, all characteristic of crustal material, are positively correlated with each other. Ozone and ash have a strong correlation, which is more likely due to meteorology than any chemical linkage (as discussed below).

[33] The autocorrelation for sodium (Figure 5) demonstrates the usefulness of this technique for investigating the lifetime of an atmospheric species. For bulk sodium with a mass mean diameter around 3 μm , there is no strong

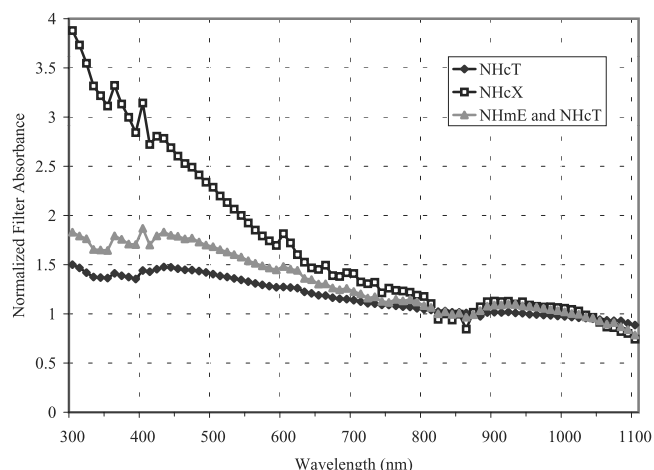


Figure 6. The normalized aerosol absorbance for the Northern Hemisphere in the NHcT (28 February to 8 March, days 59–67.5), NHcX (8–12 March, days 67.5–71) and a mixture of NHmE and NHcT (16–28 March, days 75–87) regimes. The uniformly strong absorption from 300 to 1100 nm indicates soot (elemental carbon) as the dominant light-absorbing aerosol in air that has passed over India. The strong wavelength dependence of the absorbance indicates mineral dust contributes to light absorbance by aerosol for samples collected downwind of Arabia, and may dominate in the UV.

Table 6a. Average ($\pm\sigma$) Ammonium Concentrations ($\sigma\text{g m}^{-3}$) per Size Cutoff by Meteorological Regime

Diameter Range, μm	SHmX	SHmE	NHcT	NHcX	NHc	NHmE
Number of samples	7	14	18	4	9	10
<0.48	BDL ^a	BDL	0.46 ± 0.38	0.19 ± 0.02	0.49 ± 0.29	0.11 ± 0.11
0.48–0.96	BDL	BDL	0.51 ± 0.39	0.10 ± 0.01	0.26 ± 0.19	0.14 ± 0.17
0.96–1.48	BDL	BDL	0.17 ± 0.15	0.07 ± 0.03	0.10 ± 0.05	0.04 ± 0.04
1.48–3.0	BDL	BDL	0.04 ± 0.03	0.03 ± 0.01	0.04 ± 0.03	BDL
3.0–7.2	BDL	BDL	0.05 ± 0.03	0.04 ± 0.01	0.04 ± 0.04	0.03 ± 0.03
>7.2	BDL	BDL	0.03 ± 0.02	0.03 ± 0.01	0.04 ± 0.03	BDL
Sum	BDL	BDL	1.26 ± 0.22	0.46 ± 0.06	0.98 ± 0.18	0.31 ± 0.05

^aBDL, below detection limit ($0.030 \mu\text{g m}^{-3}$).

correlation after 12 hours. For sodium particles with a diameter around $1 \mu\text{m}$, positive autocorrelation persists for 36 hours, suggesting a longer lifetime in the MBL for small sea salt particles.

[34] In the Southern Hemisphere regimes, SHmX and SHmE, the aerosol is principally of marine origin. Sea salt components comprise the majority of the aerosol mass in these regimes with negligible amounts of anthropogenic pollution. Nitrate ($0.04 \pm 0.04 \mu\text{g m}^{-3}$ in SHmX; $0.16 \pm 0.10 \mu\text{g m}^{-3}$ in SHmE) and nss-sulfate ($0.13 \pm 0.03 \mu\text{g m}^{-3}$ in SHmX; $0.36 \pm 0.10 \mu\text{g m}^{-3}$ in SHmE) concentrations are similar to previously reported values in background marine environments. *Savoie et al.* [1987] and *Rhoads et al.* [1997] reported average Southern Hemisphere nitrate values of $0.16 \pm 0.05 \mu\text{g m}^{-3}$ and $0.22 \pm 0.07 \mu\text{g m}^{-3}$ respectively and nss-sulfate values of $0.50 \pm 0.17 \mu\text{g m}^{-3}$ and $0.36 \pm 0.10 \mu\text{g m}^{-3}$ during the months of March and April in the Indian Ocean. Southern Pacific nss-sulfate values of $0.2\text{--}0.5 \mu\text{g m}^{-3}$ and nitrate values around $0.11 \mu\text{g m}^{-3}$ were reported by *Prospero and Savoie* [1989] and *Savoie et al.* [1989]. Concentrations of ammonium, calcium, and magnesium showed no evidence of contamination from continental emissions.

[35] In the three Northern Hemisphere regimes, concentrations of sulfate, nitrate, ash, nss-calcium, ammonium and nss-potassium are higher than in the Southern Hemisphere regimes (Table 3). The NHcT regime is composed of air that passed over India a few days prior to arrival at the ship. The concentrations of nss-potassium and nss-sulfate are highest in this regime. The NHcT regime has a relatively low nitrate to sulfate mass ratio of 0.47. Nitrate averages 11% and sulfate 27% of the non-sea-salt aerosol in this regime. The air from the NHcX regime has been transported from the Arabian Peninsula. This regime is the windiest, driest and coolest of any of the air masses (Table 3). The arid conditions of the Middle East result in the highest concentrations of mineral dust (ash) and nss-calcium. Nss-potassium was not detectable, providing evidence of more fossil fuel

burning than biomass burning. The nitrate to sulfate ratio is near unity, similar to that found downwind of North America indicating prevalence of fossil fuel combustion over biomass burning, although nitrate and nss-sulfate averaged only 5 and 10% of the aerosol mass. This regime has the highest ozone concentrations [*Stehr et al.*, 2002], probably because the NO_x to VOC ratio was more conducive to photochemical smog formation [*Lelieveld et al.*, 2001].

[36] As the ship cruised southwest of India, days 71–76 (12–17 March), a mixture of sources contributed to the composition of the atmosphere. Back trajectories show that air in the marine boundary layer was advected from the northwest (Arabia) while air in the lower free troposphere was advected from the northeast (India). This category, designated NHc, shows aerosol concentrations intermediate between the NHcX and NHcT regimes (Table 3); the nitrate to sulfate ratio is 0.79, halfway between the extratropical and tropical regimes. Analysis of aerosols provides evidence of a combination of sources: fossil fuel combustion (sulfate), biomass burning (nss-potassium) and wind blown mineral dust (ash and nss-calcium).

[37] Air from the NHmE regime, having spent five or more days over the Indian Ocean, has lower concentrations of most pollutants than the continental air masses. Nss-sulfate, nss-potassium, nitrate and ammonium are found in the same relative abundance, but have approximately half the concentration as in the NHcT and NHc regimes. This suggests that the NHmE air originated as continental air but has undergone depositional losses.

[38] Ammonia budget estimates [*Dentener and Crutzen*, 1994; *Zhao and Wang*, 1994] indicate that India is a major source of NH₃, and suggest that ammonia is in excess of the acids and the aerosol may be neutralized. If the degree of neutralization is defined as

$$\frac{[\text{NH}_4^+]}{2[\text{SO}_4^{2-}] + [\text{NO}_3^-]},$$

Table 6b. Average ($\pm\sigma$) Nitrate Concentrations ($\mu\text{g m}^{-3}$) per Size Cutoff by Meteorological Regime

Diameter Range, μm	SHmX	SHmE	NHcT	NHcX	NHc	NHmE
Number of samples	7	14	18	4	9	10
<0.48	BDL ^a	BDL	0.02 ± 0.16	0.03 ± 0.02	0.07 ± 0.03	0.01 ± 0.02
0.48–0.96	BDL	BDL	0.01 ± 0.06	0.01 ± 0.01	0.03 ± 0.02	0.01 ± 0.01
0.96–1.48	0.02 ± 0.01	0.01 ± 0.01	0.14 ± 0.08	0.08 ± 0.03	0.13 ± 0.04	0.06 ± 0.05
1.48–3.0	0.02 ± 0.01	0.03 ± 0.03	0.30 ± 0.14	0.12 ± 0.03	0.29 ± 0.12	0.11 ± 0.14
3.0–7.2	BDL	0.05 ± 0.04	0.68 ± 0.35	0.46 ± 0.15	0.71 ± 0.48	0.25 ± 0.27
>7.2	BDL	0.01 ± 0.01	0.34 ± 0.22	0.18 ± 0.15	0.48 ± 0.33	0.11 ± 0.10
Sum	0.04 ± 0.01	0.10 ± 0.02	1.71 ± 0.22	0.88 ± 0.16	1.71 ± 0.27	0.56 ± 0.09

^aBDL, below detection limit ($0.007 \mu\text{g m}^{-3}$).

Table 6c. Average ($\pm\sigma$) Sodium Concentrations ($\mu\text{g m}^{-3}$) per Size Cutoff by Regime

Diameter Range, μm	SHmX	SHmE	NHcT	NHcX	NHc	NHmE
Number of samples	7	14	18	4	9	10
<0.48	0.03 ± 0.02	BDL ^a	0.03 ± 0.02	0.05 ± 0.05	0.06 ± 0.03	0.05 ± 0.04
0.48–0.96	0.07 ± 0.03	BDL	0.03 ± 0.02	BDL	BDL	0.04 ± 0.02
0.96–1.48	0.32 ± 0.11	0.10 ± 0.13	0.06 ± 0.07	0.09 ± 0.05	0.09 ± 0.03	0.18 ± 0.07
1.4–3.0	0.55 ± 0.14	0.20 ± 0.19	0.16 ± 0.16	0.15 ± 0.06	0.20 ± 0.09	0.36 ± 0.20
3.0–7.2	1.21 ± 0.33	0.58 ± 0.46	0.40 ± 0.28	0.93 ± 0.47	0.78 ± 0.44	1.05 ± 0.40
>7.2	1.18 ± 0.48	0.52 ± 0.60	0.31 ± 0.37	0.53 ± 0.22	0.64 ± 0.37	0.84 ± 0.30
Sum	3.35 ± 0.52	1.43 ± 0.25	1.00 ± 0.16	1.76 ± 0.36	1.78 ± 0.33	2.52 ± 0.43

^aBDL, below detection limit ($0.029 \mu\text{g m}^{-3}$).

(where $[\text{SO}_4^{2-}]$ is nss-sulfate), then bulk aerosol in the regimes impacted by India is 64–69% neutralized, similar to boundary layer aerosol over North America. Air impacted by Arabia has lower ammonia concentrations and is only 43% neutralized. The acid-base balance in the accumulation mode will be reexamined in section 3.3.

3.2. Absorption Spectra

[39] Additional evidence of the difference between the continental tropical and the continental extratropical regimes and information on the nature of the optical properties of the aerosol can be found in the absorbance spectra (Figure 6). The absorption coefficient of the aerosols in the atmosphere (\hat{a}) during the sampling period is given by:

$$\hat{a} = \ln(R_b/R_s)/(K*V_s/A_s),$$

where V_s is the sampled air volume, A_s is the active area of the sample filter (406 cm^2 for the high-volume filters), R_b is the reflectance of the blank, R_s is the reflectance of the sample, and K is a constant that is specific to the spectral reflectance technique and the sample substrate. Intercomparisons at 565 nm with the absorbances measured concurrently with a particle soot absorption photometer (PSAP) aboard the Ron Brown (P. Quinn, NOAA Pacific Marine Environmental Laboratory, Seattle, WA 98115) indicate that, for our samples, K is 1.03 ± 0.04 ($r^2 = 0.92$). For a 1000 m^3 air sample, the 2σ standard error in the spectral reflectance measurement is about 0.4 Mm^{-1} for wavelengths greater than 400 nm, increasing to 0.6 Mm^{-1} at 360 nm and about 1 Mm^{-1} at 320 nm. Elemental carbon, a product of combustion, is a uniformly strong absorber of visible and ultraviolet radiation in the range of 300–700 nm. Mineral dust absorbs ultraviolet radiation more strongly than visible radiation. Samples collected in air from India show the uniform absorbance of elemental carbon, but the

samples from the NHcX regime show absorbance characteristic of mineral dust. The NHcX samples demonstrate the dominance of mineral dust in the NHcX regime.

3.3. Cascade Impactor Data

[40] Samples from the cascade impactors provide information on the size distribution of the aerosol particles. Averages based on particle size were calculated for each air mass classification. Nss-sulfate, nss-potassium and ammonium were found primarily on fine particles, with diameters less than $1 \mu\text{m}$ (Tables 6a–6g) with nss-sulfate dominant in all meteorological regimes. Sodium, chloride, calcium and nitrate were all found on coarse particles with diameters greater than $1 \mu\text{m}$, suggesting that these particles were composed of sea salt and wind-blown mineral dust. This difference in the composition of fine and coarse particles has been previously observed [e.g., *Li-Jones and Prospero*, 1998; *Savoie et al.*, 1987, and *Savoie and Prospero*, 1982]. As with the bulk samples, nss-potassium is highest in the regimes impacted by the Indian subcontinent.

[41] In the SHmE regime, Tables 6a–6g, the submicrometer particles primarily consist of nss-sulfate. In this relatively clean regime, with little trace of anthropogenic pollution from nss-potassium, nitrate, or ammonium, nss-sulfate is probably the result of oxidation of biogenic dimethyl sulfide (DMS) [*Ayers et al.*, 1996; *Burgermeister and Georgii*, 1991]. The coarse mode is dominated by sea salt aerosol with a peak diameter at $3 \mu\text{m}$. Nitrate levels are low but above the detection limit, and similar to those seen by *Savoie et al.* [1987] and *Savoie and Prospero* [1982].

[42] The sea salt concentration and size distribution in the NHcT regime, was similar to the SHmE, but the concentration of nss-sulfate on the submicrometer particles was ten times greater; the relative increase in ammonium was even larger. The mode for ammonium sulfate was $0.48 \mu\text{m}$ and potassium showed a similar size distribution. NHmE dis-

Table 6d. BDL Average ($\pm\sigma$) Non-Sea-Salt Sulfate ($\mu\text{g m}^{-3}$) per Size Cutoff by Meteorological Regime

Diameter Range, μm	SHmX	SHmE	NHcT	NHcX	NHc	NHmE
Number of samples	7	14	18	4	9	10
<0.48	0.14 ± 0.02	BDL ^a	1.60 ± 0.95	0.55 ± 0.08	1.34 ± 0.48	0.62 ± 0.51
0.48–0.96	0.02 ± 0.02	BDL	1.95 ± 1.01	0.26 ± 0.09	0.99 ± 0.49	0.57 ± 0.66
0.96–1.48	BDL	BDL	0.54 ± 0.33	0.13 ± 0.04	0.27 ± 0.11	0.19 ± 0.16
1.4–3.0	BDL	BDL	0.07 ± 0.05	0.03 ± 0.06	0.05 ± 0.04	0.03 ± 0.04
3.0–7.2	BDL	BDL	0.05 ± 0.08	BDL	0.04 ± 0.08	BDL
>7.2	BDL	BDL	0.02 ± 0.05	BDL	BDL	BDL
Sum	0.16 ± 0.02	BDL	4.23 ± 0.86	0.98 ± 0.23	2.69 ± 0.59	1.40 ± 0.29

^aBDL, below detection limit ($0.020 \mu\text{g m}^{-3}$).

Table 6e. Average ($\pm\sigma$) Total Calcium Concentrations ($\mu\text{g m}^{-3}$) per Size Cutoff by Meteorological Regime

Diameter Range, μm	SHmX	SHmE	NHcT	NHcX	NHc	NHmE
Number of samples	7	14	18	4	9	10
<0.48	BDL ^a	BDL	0.03 ± 0.02	0.02 ± 0.03	0.02 ± 0.04	0.02 ± 0.02
0.48–0.96	BDL	BDL	0.02 ± 0.02	BDL	0.02 ± 0.01	BDL
0.96–1.48	0.03 ± 0.01	0.02 ± 0.01	0.02 ± 0.02	0.03 ± 0.02	0.03 ± 0.01	0.02 ± 0.01
1.4–3.0	0.04 ± 0.01	BDL	0.03 ± 0.03	0.03 ± 0.02	0.05 ± 0.04	0.04 ± 0.02
3.0–7.2	0.07 ± 0.03	0.02 ± 0.03	0.08 ± 0.05	0.12 ± 0.01	0.17 ± 0.09	0.09 ± 0.03
>7.2	0.08 ± 0.06	0.02 ± 0.03	0.05 ± 0.04	0.06 ± 0.03	0.12 ± 0.08	0.07 ± 0.03
Sum	0.24 ± 0.09	0.06 ± 0.09	0.23 ± 0.14	0.26 ± 0.02	0.41 ± 0.18	0.24 ± 0.09

^aBDL, below detection limit ($0.02 \mu\text{g m}^{-3}$).

tributions are similar to NHcT, but the concentrations are reduced to one-third of those in the continental regime probably due to depositional losses in transit over the ocean.

[43] The NHcX regime has a size distribution similar to that in the NHcT regime except potassium seems to come primarily from sea salt. The nss-potassium we can detect is in the accumulation mode. The absolute concentration of sulfate is lower than in the NHcT regime because the sources are farther away, providing additional time for dilution and removal processes to occur. In the mixed regime, NHc, sulfate concentrations are intermediate between NHcX and NHcT. Mineral dust from both India and Arabia contribute to the high concentrations of calcium.

[44] The cascade impactor samples show that sulfate, potassium and ammonium are found primarily on the submicrometer particles. The nitrate, having been deposited initially onto alkaline sea salt aerosol, is found in the coarse mode (particle diameters greater than $1 \mu\text{m}$), and should not be included in acid-base balance of accumulation mode particles. When we define the degree of neutralization as

$$\frac{[\text{NH}_4^+] + [\text{K}^+]}{2[\text{SO}_4^{2-}]}$$

The aerosol from Arabia is 75% neutralized. The NHcT and NHmE regimes show an average ratio near unity (Table 4). The NHc regime shows net alkalinity. *Dentener and Crutzen* [1994] suggest that nitrous oxide (N_2O) can be generated in the reaction between the NH_2 radical, an intermediate in the removal of NH_3 by OH, and NO_2 (at concentrations greater than 300 ppt). Acidic aerosol containing sulfate can drive ammonia out of the gas phase and into the aerosol phase, leaving open the possibility of excess ammonia and the in situ production of N_2O [*Dentener, 1993*].

[45] Bicarbonate-carbonate buffering complicates the acid-base chemistry of sea salt aerosol. There appears to be enough nitrate to neutralize the inherent alkalinity of sea salt, based on an average value of 1.3 for the ratio of the sum of chloride and nitrate to sodium in the coarse mode aerosol of the Northern Hemisphere. Heterogeneous reactions involving the release of halogens are acid catalyzed [*Dickerson et al., 1999*]. Measurements of precipitation chemistry taken from the ships indicate weakly acidic rain; the pH varied from 4.8 to 5.3 [*Granat et al., 2002*] providing supporting evidence that aged sea salt aerosols have a pH below 7.

3.4. Comparison to Other INDOEX Observations

[46] During INDOEX, aerosol measurements were also performed from a C-130 aircraft [*Lelieveld et al., 2001*] and at KCO, 500 km southwest of India [*Chowdhury et al., 2001*]. Measurements from all three platforms showed heavy aerosol loading. Reconstructed aerosol mass was calculated from the sum of the measured species, with total organic material obtained by multiplying organic carbon by a factor of 1.5 [*Wolff et al., 1991*]. The average total mass was $17 \mu\text{g m}^{-3}$ from KCO compared to a reconstructed mass of $19.7 \mu\text{g m}^{-3}$ onboard the ship in air from India (NHcT regime). Ammonium comprised 7% of the total aerosol mass from the aircraft and 7–9% at KCO, very similar to the percent mass of ammonium as measured from the ship (7%). The sulfate percentages also showed good agreement with averages of 9% from the aircraft, 7–9% at KCO and 7% from the ship.

[47] There was greater discrepancy between measurements of coarse particles since sampling from the C-130 and KCO focused on collecting and characterizing particulate matter with aerodynamic diameter (D_a) < $1.8 \mu\text{m}$. Nitrate accounted for 1 and 1.7% of total aerosol measured from the C-130 and KCO respectively but nitrate accounted for 9% of the total (bulk) aerosol measured with high-volume samplers on the ship. The techniques employed for

Table 6f. Average ($\pm\sigma$) Non-Sea-Salt Calcium Concentrations ($\mu\text{g m}^{-3}$) per Size Cutoff by Meteorological Regime

Diameter Range, μm	SHmX	SHmE	NHcT	NHcX	NHc	NHmE
Number of samples	7	14	18	4	9	10
<0.48	BDL ^a	BDL	0.02 ± 0.02	BDL	BDL	BDL
0.48–0.96	BDL	BDL	0.02 ± 0.02	BDL	BDL	BDL
0.96–1.48	BDL	BDL	0.02 ± 0.02	0.02 ± 0.02	0.02 ± 0.01	BDL
1.48–3.0	0.02 ± 0.01	BDL	0.03 ± 0.02	0.02 ± 0.02	0.05 ± 0.04	0.02 ± 0.01
3.0–7.2	0.03 ± 0.02	BDL	0.06 ± 0.04	0.09 ± 0.01	0.14 ± 0.08	0.05 ± 0.03
>7.2	0.04 ± 0.07	BDL	0.04 ± 0.04	0.04 ± 0.03	0.09 ± 0.08	0.04 ± 0.02
Sum	0.09 ± 0.01	BDL	0.19 ± 0.16	0.17 ± 0.03	0.30 ± 0.05	0.11 ± 0.01

^aBDL, below detection limit ($0.02 \mu\text{g m}^{-3}$).

Table 6g. Average ($\pm\sigma$) Non-Sea-Salt Potassium Concentrations ($\mu\text{g m}^{-3}$) per Size Cutoff by Regime

Diameter Range, μm	SHmX	SHmE	NHcT	NHcX	NHc	NHmE
Number of samples	7	14	18	4	9	10
<0.48	BDL ^a	BDL	0.09 \pm 0.06	0.01 \pm 0.002	0.07 \pm 0.03	0.02 \pm 0.03
0.48–0.96	BDL	0.01 \pm 0.01	0.09 \pm 0.06	0.01 \pm 0.004	0.06 \pm 0.03	0.03 \pm 0.03
0.96–1.48	BDL	BDL	0.03 \pm 0.02	0.003 \pm 0.003	0.02 \pm 0.01	0.01 \pm 0.01
1.4–3.0	BDL	BDL	0.01 \pm 0.004	BDL	0.004 \pm 0.003	BDL
3.0–7.2	BDL	BDL	0.01 \pm 0.01	BDL	0.01 \pm 0.01	BDL
>7.2	BDL	BDL	BDL	BDL	BDL	BDL
Sum	BDL	0.01 \pm 0.01	0.23 \pm 0.04	0.02 \pm 0.002	0.16 \pm 0.03	0.06 \pm 0.01

^aBDL, below detection limit (0.003 $\mu\text{g m}^{-3}$).

our measurements appear to have a greater recovery of particles in the coarse mode. Cascade impactor data show maximum nitrate concentrations at $D_a = 3.0 \mu\text{m}$ (Table 6b).

4. Conclusions

[48] Five air masses types were encountered during the INDOEX cruise. The Southern Hemisphere air masses, SHmX and SHmE, have aerosol concentrations typical of marine background levels. The northern Indian Ocean was impacted by air masses from India, Arabia, or both.

[49] Our measurements show high concentrations of nitrate associated with the coarse-mode sea salt aerosol not observed in other INDOEX measurements focusing on the fine mode aerosol. Throughout the Northern Hemisphere over the Indian Ocean, there was enough nitrate to reduce the pH of sea salt aerosol below 7, allowing for the possibility of release of halogens into the gas phase where they destroy ozone and other species.

[50] The NHcT air mass, which originated over India, showed evidence of biomass burning, fossil fuel combustion and mineral dust; it contained the highest concentrations of nss-sulfate, ammonium and nss-potassium. These species were mostly found on the fine particles. The sulfate was generally neutralized by the combination of ammonium and potassium. Soot appeared to dominate the absorption of radiation by aerosols.

[51] Air polluted by transport over the Arabian Peninsula, the NHcX regime, displayed evidence of mineral dust and fossil fuel burning rather than biomass burning as in air from India. The nitrate to sulfate ratio was higher and the aerosol more acidic. Mineral dust played an important role in absorption of radiation by aerosols.

[52] Statistical analysis was unable to definitively distinguish between fossil fuel combustion and biomass burning as the source of black carbon from India. Black carbon correlated strongly with markers for both fossil and bio-fuels, suggesting a combination of the two sources or some unaccounted-for process at play.

[53] **Acknowledgments.** This work was supported by NSF through the Center for Clouds, Chemistry and Climate, the INDOEX program (ATM-9612893) and fellowship stipend support from the National Physical Science Consortium and NASA. The authors wish to thank the Pacific Marine Environmental Laboratory of NOAA for compiling back trajectories and the captain and crew of the NOAA R/V *Ronald H. Brown* for their invaluable assistance.

References

Ahrens, C. D., *Meteorology Today*, 528 pp., Brooks/Cole, Pacific Grove, Calif., 2000.

- Andreae, M. O., and P. J. Crutzen, Atmospheric aerosols: Biogeochemical sources and role in atmospheric chemistry, *Science*, 276(5315), 1052–1058, 1997.
- Ayers, G. P., J. M. Caaney, H. Granek, and C. Leck, Dimethylsulfide oxidation and the ratio of methanesulfonate to non-sea-salt sulfate in the marine aerosol, *J. Atmos. Chem.*, 25, 307–325, 1996.
- Burgermeister, S., and H. W. Georgii, Distribution of methanesulfonate, nss-sulfate and dimethylsulfide over the Atlantic and the North Sea, *Atmos. Environ.*, 25, 587–595, 1991.
- Chowdhury, Z., L. S. Hughes, L. G. Salmon, and G. R. Cass, Atmospheric particle size and composition measurements to support light extinct calculations over the Indian Ocean, *J. Geophys. Res.*, 106, 28,597–28,605, 2001.
- Dentener, F. J., Heterogeneous chemistry in the troposphere, Ph.D. dissertation, Univ. Utrecht, Utrecht, Netherlands, 1993.
- Dentener, F. J., and P. J. Crutzen, A 3-dimensional model of the global ammonia cycle, *J. Atmos. Chem.*, 19(4), 331–369, 1994.
- Dickerson, R. R., K. P. Rhoads, T. P. Carsey, S. J. Oltmans, and P. J. Crutzen, Ozone in the remote marine boundary layer: A possible role for halogens, *J. Geophys. Res.*, 104, 21,385–21,395, 1999.
- Dickerson, R. R., M. O. Andreae, T. Campos, O. L. Mayol-Bracero, C. Neusuess, and D. G. Streets, Analysis of black carbon and carbon monoxide observed over the Indian Ocean: Implications for emissions and photochemistry, *J. Geophys. Res.*, 107(D19), 8017, doi:10.1029/2001JD000501, 2002.
- Draxler, R. R., The accuracy of trajectories during ANATEX calculated using dynamic model analysis versus rawinsonde observations, *J. Appl. Meteorol.*, 30, 1466–1467, 1991.
- Erickson, D. J., and R. A. Duce, On the global flux of atmospheric sea salt, *J. Geophys. Res.*, 93, 14,079–14,088, 1988.
- Fitzgerald, J. W., Marine aerosols: A review, *Atmos. Environ.*, 25, 533–545, 1991.
- Galanter, M., H. Levy, and C. R. Carmichael, Impacts of biomass burning on tropospheric CO, NO_x and O₃, *J. Geophys. Res.*, 105(D5), 6633–6653, 2000.
- Glickman, T. S., (Ed.), *Glossary of Meteorology*, 2nd ed., 855 pp., Am. Meteorol. Soc., Boston, Mass., 2000.
- Granat, L., M. Norman, C. Leck, U. C. Kulshrestha, and H. Rodhe, Wet scavenging of sulfur compounds and other constituents during the Indian Ocean Experiment (INDOEX), *J. Geophys. Res.*, 107(D19), 8025, doi:10.1029/2001JD000499, 2002.
- Howell, S., A. P. Pszenny, P. Quinn, and B. Huebert, A field intercomparison of three cascade impactors, *Aerosol Sci. Technol.*, 29, 475–492, 1998.
- Jha, B., and T. N. Krishnamurti, Real-time meteorological atlas during the INDOEX-1999, *FSU Rep. 99-09*, Fla. St. Univ., Tallahassee, Fla., 1999.
- Johansen, A. M., R. L. Siefert, and M. R. Hoffmann, Chemical characterization of ambient aerosol collected during the southwest monsoon and intermonsoon seasons over the Arabian Sea: Anions and cations, *J. Geophys. Res.*, 104, 26,325–26,347, 1999.
- Keene, W. C., A. P. Pszenny, J. N. Galloway, and M. E. Hawley, Sea-salt corrections and interpretation of constituent ratios in marine precipitation, *J. Geophys. Res.*, 91, 6647–6658, 1986.
- Krishnamurti, T. N., B. Jha, P. J. Rasch, and V. Ramanathan, High-resolution global reanalysis highlighting the winter monsoon, part I: Reanalysis field, *Meteorol. Atmos. Phys.*, 64, 123–150, 1997.
- Lal, S., M. Naja, and A. Jayaraman, Ozone in the marine boundary layer over the tropical Indian Ocean, *J. Geophys. Res.*, 103, 18,907–18,917, 1998.
- Lelieveld, J., et al., The Indian Ocean Experiment: Widespread air pollution from South and Southeast Asia, *Science*, 291, 1031–1035, 2001.
- Li-Jones, X., and J. M. Prospero, Variations in the size distribution of non-sea-salt sulfate aerosol in the marine boundary layer at Barbados: Impact of African dust, *J. Geophys. Res.*, 103, 16,073–16,084, 1998.

- Maring, H., D. L. Savoie, and M. A. Izaguirre, Aerosol physical and optical properties and their relationship to aerosol composition in the free troposphere at Izana, Tenerife, Canary Islands, during July 1995, *J. Geophys. Res.*, *105*(D11), 14,677–14,700, 2000.
- Neusuess, C., T. Gnauk, A. Plewka, H. Herrmann, and P. K. Quinn, Carbonaceous aerosol over the Indian Ocean: OC/EC fractions and selected specifications from size-segregated onboard samples, *J. Geophys. Res.*, *107*(D19), 8031, doi:10.1029/2001JD000327, 2002.
- Olivier, J. G. J., A. F. Bouwman, C. W. M. Vandermaas, and J. J. M. Berdowski, Emission Database for Global Atmospheric Research (EDGAR), *Environ. Monit. Assess.*, *31*(1–2), 93–106, 1994.
- Parameswaran, K., P. R. Nair, R. Rajan, and M. V. Ramana, Aerosol loading in coastal and marine environments in the Indian Ocean during winter season, *Curr. Sci.*, *76*(7), 947–955, 1999.
- Parashar, D. C., U. C. Kulshrestha, and C. Sharma, Anthropogenic emissions of NO_x, NH₃ and N₂O in India, *Nutr. Cyc. Agroecosys.*, *52*(2–3), 255–259, 1998.
- Parsons, R. L., and R. R. Dickerson, NOAA ship *Ronald H. Brown*: Study global climate variability, *Sea Technol.*, *40*(6), 39–45, 1999.
- Prospero, J. M., and D. L. Savoie, Effect of continental sources on nitrate over the Pacific Ocean, *Nature*, *339*, 687–689, 1989.
- Pszenny, A. A. P., Particle size distributions of methanesulfonate in the tropical marine boundary layer, *J. Atmos. Chem.*, *14*, 273–284, 1992.
- Quinn, P. K., D. J. Coffman, V. N. Kapustin, T. S. Bates, and D. S. Covert, Aerosol optical properties in the marine boundary layer during the First Aerosol Characterization Experiment (ACE 1) and the underlying chemical and physical aerosol properties, *J. Geophys. Res.*, *103*, 16,547–16,563, 1998.
- Quinn, P. K., D. J. Coffman, T. S. Bates, T. L. Miller, J. E. Johnson, E. J. Welton, C. Neusuess, M. Miller, and P. J. Sheridan, Aerosol optical properties during INDOEX 1999: Means, variability, and controlling factors, *J. Geophys. Res.*, *107*(D19), 8020, doi:10.1029/2000JD000037, 2002.
- Rhoads, K. P., P. Kelley, R. R. Dickerson, T. P. Carsey, M. Farmer, D. L. Savoie, and J. M. Prospero, Composition of the troposphere over the Indian Ocean during the monsoonal transition, *J. Geophys. Res.*, *102*, 18,981–18,995, 1997.
- Rosby, C. G., Thermodynamics applied to air mass analysis, *Tech. Rep. 3*, Mass. Inst. Technol., Cambridge, Mass., 1932.
- Savoie, D. L., and J. M. Prospero, Particle size distribution of nitrate and sulfate in the marine atmosphere, *Geophys. Res. Lett.*, *9*, 1207–1210, 1982.
- Savoie, D. L., J. M. Prospero, and R. T. Nees, Nitrate, non-sea-salt sulfate, and mineral aerosol over the northwestern Indian Ocean, *J. Geophys. Res.*, *92*, 933–942, 1987.
- Savoie, D. L., J. M. Prospero, J. T. Merrill, and M. Uematsu, Nitrate in the atmospheric boundary layer of the tropical South Pacific: Implications regarding sources and transport, *J. Atmos. Chem.*, *8*, 391–415, 1989.
- Savoie, D. L., J. M. Prospero, S. J. Oltmans, W. C. Graustein, K. K. Turekian, J. T. Merrill, and H. Levy II, Sources of nitrate and ozone in the marine boundary layer of the tropical North Atlantic, *J. Geophys. Res.*, *97*(D11), 11,575–11,589, 1992.
- Seinfeld, J. H., and S. N. Pandis, *Atmospheric Chemistry and Physics*, John Wiley, New York, 1998.
- Siefert, R. L., A. M. Johansen, and M. R. Hoffman, Chemical characterization of ambient aerosol collected during the southwest monsoon and intermonsoon seasons over the Arabian Sea: Labile Fe(II) and other trace metals, *J. Geophys. Res.*, *104*, 3511–3526, 1999.
- Smith, K. R., Air Pollution—Assessing total exposure in developing countries, *Environment*, *30* (10), 16–20, 28–35, 1998.
- Stehr, J. W., W. P. Ball, R. R. Dickerson, B. G. Doddridge, C. A. Piety, and J. E. Johnson, Latitudinal gradients in O₃ and CO during INDOEX 1999, *J. Geophys. Res.*, *107*(D19), 8016, doi:10.1029/2001JD000446, 2002.
- Streets, D. G., and S. T. Waldhoff, Biofuel use in Asia and acidifying emissions, *Energy*, *23*(12), 1029–1042, 1998.
- Streets, D. G., and S. T. Waldhoff, Greenhouse gas emissions from biofuel combustion in Asia, *Energy*, *24*(10), 841–855, 1999.
- Wolff, G. T., M. S. Ruthkosky, D. P. Stroup, and P. E. Korsog, A characterization of the principal PM-10 species in Claremont (summer) and Long Beach (fall) during SCAQS, *Atmos. Environ., Part A*, *25*, 2173–2186, 1991.
- Zhao, D. W., and A. P. Wang, Estimation of anthropogenic ammonia emissions in Asia, *Atmos. Environ.*, *28*(4), 689–694, 1994.

W. Ball, Department of Chemistry, University of Maryland, College Park, MD 20742, USA. (ball@atmos.umd.edu)

T. Carsey, NOAA-AOML, 4301 Rickenbacker Causeway, Miami, FL 33149, USA. (carsey@aoml.noaa.gov)

R. Dickerson, B. Doddridge, and J. Stehr, Department of Meteorology, University of Maryland, College Park, MD 20742, USA. (russ@atmos.umd.edu; bruce@atmos.umd.edu; stehr@atmos.umd.edu)

T. Miller, NOAA-PMEL, 7600 Sand Point Way NE, Seattle, WA 98115, USA. (tmiller@pmel.noaa.gov)

D. Savoie, RSMAS/MAC, University of Miami, 4600 Rickenbacker Causeway, Miami, FL 33149, USA. (dsavoie@rsmas.miami.edu)